ELSEVIER

Journal of Alloys and Compounds 349 (2003) 255–263

Journal of ALLOYS AND COMPOUNDS

www.elsevier.com/locate/jallcom

Effect of extended ball milling on graphite

N.J. Welham[a,*], V. Berbenni[b], P.G. Chapman[c]

[a]*Department of Electronic Materials Engineering and Department of Applied Mathematics, Research School of Physical Sciences and Engineering, Australian National University, Canberra, ACT 0200, Australia*

[b]*CSGI—Dipartimento di Chimica Fisica dell'Università di Pavia, Viale Taramelli, 16-27100 Pavia, Italy*

[c]*School of Applied Chemistry, Curtin University of Technology, Kent Street, Bentley, WA 6102, Australia*

Received 3 June 2002; accepted 14 June 2002

Abstract

Graphite has been milled for up to 1000 h in a laboratory scale tumbling ball mill under vacuum. Raman spectroscopy of the powders indicated the increasing dominance of D-type graphitic sp^2 bonding over G-type bonding with increasing milling time. Diamond-like sp^3 bonding and possibly fullerene-like bonding also became evident after milling. TEM of the 100 h sample showed the presence of ribbons which were composed of sheets showing defects, delamination, translation, warping and curvature. Interplanar spacings of 0.40–0.50 nm were measured with the spacing increasing towards the edge of the ribbons where delamination was evident. Thermogravimetric analysis in argon of the powder after exposure to air showed an increasing mass loss with milling time indicating the presence of chemisorbed gas. Using TG–FTIR the gas was found to be a mixture of CO_2 and an unidentified gas (probably oxygen). BET surface area measurements showed a maximum in the surface area; however, this was shown to be massively in error for the longer milling times due to the presence of the chemisorbed gas.

Keywords: Disordered systems; Amorphisation; Thermal analysis; SEM; TEM

1. Introduction

Mechanical processing of powders has been studied extensively in recent years with the growing interest in nanocrystalline materials and their unusual properties. The changes in the crystallinity of graphite during milling has been examined on several occasions [1–8] and the general conclusion is that graphite passes through a nanocrystalline phase prior to amorphisation. Although a wide range of mechanochemical or mechanically activated reactions involving carbon have been reported [9–21], there has been surprisingly little study on the subsequent physical properties of the carbon itself. This is especially surprising given the results from a range of milled materials indicating enhanced reactivity after extended milling [22–30] and the global industrial importance of carbon.

Milling of graphite in different atmospheres has been shown [7] to lead to significantly different BET surface areas. After 10 h milling, the area obtained in an argon atmosphere was greater than in air and much greater than in oxygen [7]. However, no data was presented on the mass loss in an inert atmosphere during heating and the difference may simply be attributed to adsorption of oxygen as graphite is substantially more reactive towards oxygen after milling [7,8,31]. Increased intercalation of lithium ions has also been reported for milled graphite [7,32]. Several publications [7,8,31–33] have measured the BET surface area of milled carbons and all report that a maximum occurs for graphite. However, thermogravimetric analysis in argon of graphite milled in vacuum for up to 1000 h showed that there was a substantial fraction of gas (up to 0.5 g gas/g graphite) strongly adsorbed onto the surface [31]. This result brings into severe doubt the values of the surface area measured as nitrogen is assumed to adsorb only onto gas-free surfaces. The claim that milling graphite produces nanoporous carbon [33] based entirely on nitrogen adsorption is clearly wrong.

This paper examines the effect of extended ball milling on the properties of graphite.

*Present address: Mineral Science, Murdoch University, Perth, WA 6150, Australia.

E-mail address: nicholas.welham@murdoch.edu.au (N.J. Welham).

0925-8388/02/$ – see front matter
PII: S0925-8388(02)00880-0

2. Experimental

Samples (7 g) of graphite (nominally >99.9% C) were ball milled at room temperature under vacuum ~10^{-2} Pa for 100 and 1000 h in a laboratory tumbling ball mill [34]. After the allotted time the mills were opened, the powders were scraped out and placed into loosely capped containers to allow equilibration with air.

Thermogravimetric analyses (TGA) were performed using a Shimadzu TGA-50 at a heating rate of 20 °C min^{-1} up to 1200 °C where the sample was held for 1 h. These runs were made using a 100 ml min^{-1} flow of dried argon. The mass loss at 1200 °C was modelled as a function of time and the fitted curve extrapolated to estimate the total mass of adsorbed gas.

TGA–FTIR measurements were made using a DuPont 951 TGA at a heating rate of 20 °C min^{-1} up to about 860 °C, the maximum temperature of this instrument. The samples were purged with dried nitrogen flowing at 100 ml min^{-1} for 3 h prior to heating to remove free water and reduce the CO_2 introduced into the system during loading. The nitrogen flow continued throughout the heating and swept any evolved gas into a gas cell fitted within a Nicolet 730 FTIR. The gas lines and cell were heated to 200 °C throughout the entire run to prevent condensation of water within the system. A lag of approximately 1 min was evident between the mass loss and the FTIR detecting the evolved gas. This was due to the volume of the transfer system between the TGA pan and the gas cell. This lag has not been corrected for in the diagrams presented below. The IR spectra of the evolved gases were recorded in absorbance mode at a resolution of 8 cm^{-1} using 16 co-added interferograms per measurement.

Due to the extremely high infra-red absorbance of the carbon, FTIR measurements were made using an MTEC Photoacoustic model 200 accessory mounted in a Bruker IFS 66 FTIR. The photoacoustic cell was purged using high purity helium immediately prior to measurement and the FTIR was continuously purged with dried CO_2 free air. The data was collected by co-adding 256 scans at a resolution of 4 cm^{-1} over the range of 1000–4000 cm^{-1}. The background spectrum used was that from C198 carbon lamp black collected under identical conditions to the samples.

Raman spectra were obtained using a Renishaw model 2000 instrument over the range 800–2000 cm^{-1}. No preparation of powders was made with the as-milled powders simply imaged under the microscope, this method was found to be representative with replicate sample areas showing identical Raman response. The source was a near infrared (NIR) laser operating at 780 nm at a power of 10 mW. The data obtained were fitted by mixed Gaussian–Lorentzian peaks.

The surface area of the powders was determined by multipoint nitrogen adsorption using a Micromeritics Gemini system. Samples were prepared by heating up to 200 °C under vacuum for 24 h prior to measurement. The internal (micropore) area and external surface area were determined by the Harkins and Jura method [35] and their sum was identical to the area determined separately by the BET method [36].

Transmission electron microscopy was performed at 100 kV in a Philips 430 TEM using samples dispersed in alcohol and dropped onto uncoated copper grids.

3. Results

Raman spectra of the milled graphite are shown in Fig. 1. After heating the samples for 1 h at 1200 °C in an argon atmosphere the spectra were indistinguishable from those of the as-milled powders indicating that there was no graphitisation under these conditions.

Fitting of the data was found to require five Lorentzian peaks, as shown for the as-milled 1000 h powder in Fig. 1. These peaks were at 1166±32, 1309±7, 1473±29, 1573±22 and 1607±14 cm^{-1} ($\pm 2\sigma$), although the peak at 1473 cm^{-1} was absent in the unmilled powder. The peaks at 1309 cm^{-1} and 1573 cm^{-1} are the well known graphite D- and G-peaks which relate to graphitic sp^2-bonding. The lower of these is not observed in single crystal graphite as it is associated with structural disordering and its position is reported to change with excitation wavelength [37]. Combining reported peak positions (1355 cm^{-1} when using the 514.5 nm Ar-ion laser line and 1330 cm^{-1} with the 632.8 nm HeNe line [37]) with the position here

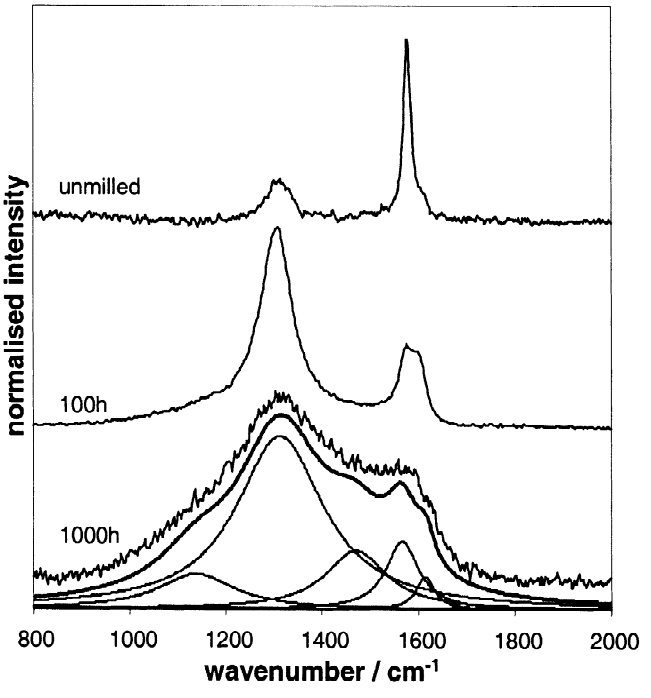

Fig. 1. Raman spectra of the unmilled and milled graphite powders. The fit for the 1000 h milled powder is shown.

indicates a linear decrease in the peak position with increasing excitation wavelength:

$$\text{D-peak position} = 1441.9 - 0.1720\,\lambda \quad r^2 = 0.994$$

The peak at 1607 cm^{-1} is associated with the initial stages of disordering and is present in most Raman spectra of graphite [37]. The peak at 1166 cm^{-1} can be attributed to sp^3-bonded amorphous diamond [38–40], the peak at 1473 cm^{-1} does not seem to have been reported previously. This latter peak may be due to fullerene-like structures in the carbon which have a large number of possible Raman modes depending upon the size and bonding of the carbon atoms [41,42].

The mass loss of the milled graphite powders during TGA are shown in Fig. 2. Holding the samples at 1200 °C showed a slow decay in the rate of mass loss with time. This was modelled using an exponential fit and the estimated mass loss at infinite time is shown by the squares in Fig. 2.

The differential of a separate TGA trace up to 860 °C is plotted in Fig. 3 with the concomitant evolution of CO_2. Up to ~200 °C the mass loss does not follow the same trend as the CO_2 evolution. This is not unexpected as it is known that water is the major mass loss during this temperature range. The water loss was somewhat more extensive for the 1000 h milled powder than for the shorter milling times, indicating that the 1000 h sample must have contained more adsorbed water than the other two powders after equilibration in air.

For all samples evolution of CO_2 is clearly evident above ~100 °C. The CO_2 evolution and DTGA plots

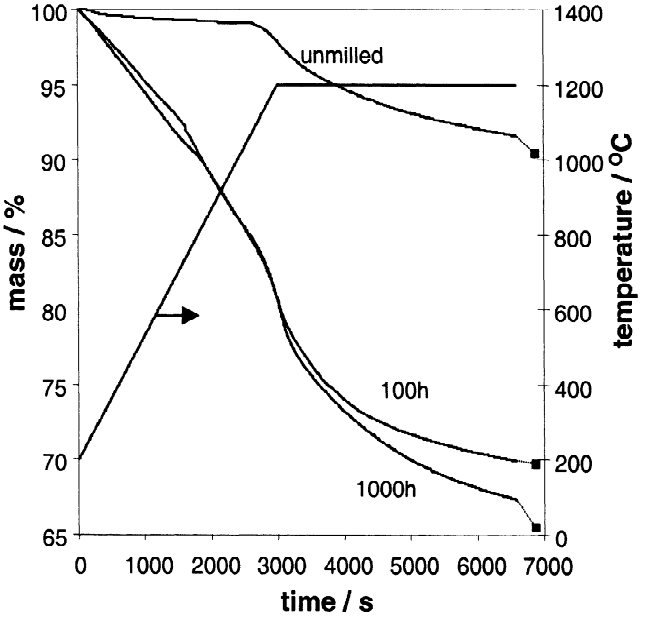

Fig. 2. TGA traces of graphite milled for 0, 100 and 1000 h heated at 20 °C min^{-1} to 1200 °C where the samples were held for 1 h. The squares are the estimated mass loss were the heating to be continued indefinitely.

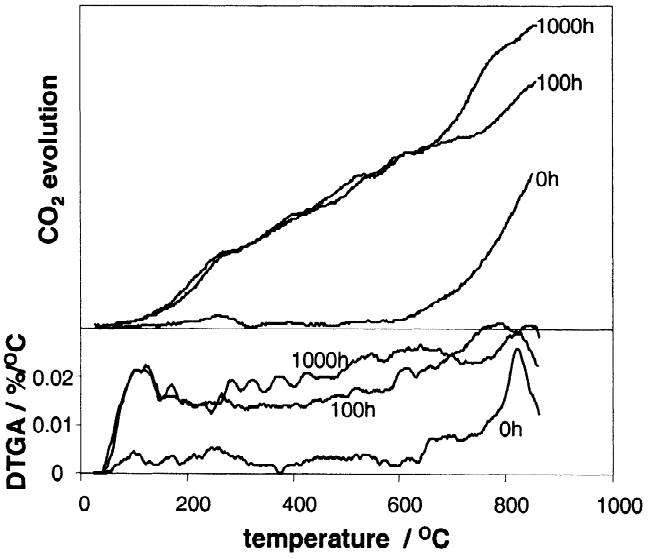

Fig. 3. Differentiated TGA traces and evolution of carbon dioxide as a function of temperature.

follow similar trends for all three milling times, this most obvious for the 1000 h milled powder where a sudden mass loss event was mirrored by an increase in CO_2 evolution. Integration of the CO_2 evolution curve enabled comparison of the CO_2 evolution with the total mass loss during heating. These values, presented in Table 1, are normalised with respect to the unmilled powder.

The increase in mass loss and CO_2 evolved is similar for the 100 h powder indicating that the mass loss increase was mainly due to CO_2. For the 1000 h milled powder the mass loss increase is almost double the increase in CO_2 evolved; clearly, there is another gas evolving. FTIR did not detect any other gas until around 800 °C where CO became evident. This is most probably due to reaction between the CO_2 and carbon which is thermodynamically favourable at >700 °C and not due to evolution of CO from the surface of the solid.

A chemical reaction between O_2 and an active carbon surface has been shown to occur [43] forming CO and CO_2. In this case it seems that CO_2 was certainly formed, CO may have been formed and dissociated into C and CO_2 at low temperatures. It is certain that other gases were evolved during heating. The most likely candidate is oxygen since this is not detectable by IR.

Initially, it was suspected that the mass loss may have partially been due to adventitious oxygen in the nitrogen

Table 1
Ratio of mass loss and total CO_2 evolution of the powders heated to 860 °C

Milling time/h	Mass	CO_2
0	1.00	1.00
100	1.24	1.30
1000	2.40	1.75

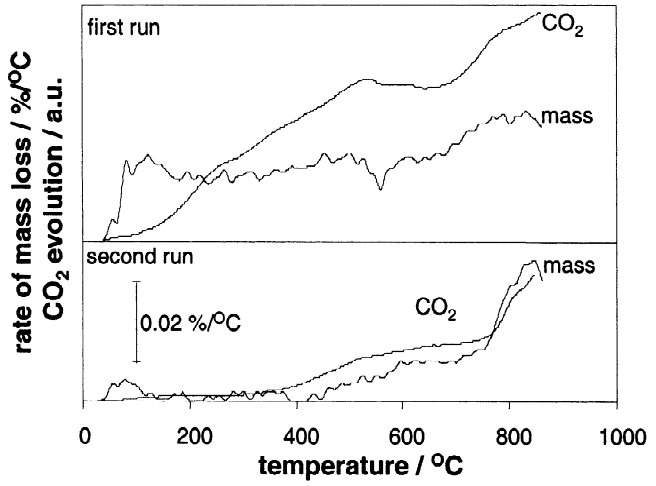

Fig. 4. Differentiated TGA traces and evolution of carbon dioxide as a function of temperature for 1000 h milled AC, sample heated in nitrogen, allowed to cool to room temperature then heated again.

stream causing some oxidation to CO_2. This can be discounted by examining Fig. 4 which shows the traces for a sample of the 1000 h milled powder which was heated, allowed to cool and then heated again, all with the nitrogen flowing.

Had adventitious oxygen been responsible for the mass loss then a similar mass loss in both runs would have been expected; clearly, this is not the case. The mass loss during the first heating run shows a peak for water, centred at ~100 °C. After this, the mass loss rate increased slightly until ~670 °C when a rapid mass loss event was evident. These events are mirrored in the CO_2 trace with no CO_2 evolving until ~120 °C; then an increased evolution until a sudden release of CO_2 occurred.

The second heating run produced a close correlation between the mass loss rate and CO_2 evolution. Unlike the first run, there was no evidence of water during the initial heating; this is not unexpected as the nitrogen flowing throughout was dried. The start of CO_2 evolution was ~200 °C with an associated mass loss. This continued until ~720 °C where a sudden mass loss and concomitant increase in CO_2 evolution were evident. Integration of the mass loss and CO_2 evolution showed that the mass loss in the second run was 32% of that in the first run and the CO_2 evolved was 34% of that of the first run. This clearly, demonstrates that the mass loss in the second run was entirely due to CO_2. The heating–cooling cycle was repeated four times beyond which no further mass loss occurred, implying that all of the gas had been removed from the carbon. The mass remaining was 20.7% of the original mass, a similar final mass was recorded in both argon and nitrogen, indicating that the adsorbed gas could not have been nitrogen.

Thus, it would seem that the difference in mass loss between the samples can only be due to difference in the gas content of the powders; the longer milled powders containing more gas than the shorter milled powders. The increasing mass loss with temperature would imply that there was a range of bond strengths between the gas and carbon. The presence of peaks for CO_2 evolution would suggest that there was a larger fraction of a particular bond strength than most.

During the second heating, there is a mass loss with an associated peak for CO_2 evolution at ~750 °C which was completely absent after the first run. It has been shown [44] that partial recovery of damage to graphite induced during milling is recovered by heating. The more strongly bound sites also get partially annealed out allowing more of the gas to evolve at lower temperatures during the second run.

The absence of oxygen was also confirmed by the identical mass loss up to 1100 °C of a sample run using a flowing atmosphere of 5% hydrogen in argon. Above 1100 °C the sample run in hydrogen lost mass more rapidly; presumably this was due to reaction between the hydrogen and carbon.

Photoacoustic FTIR spectra of the unmilled and 1000 h milled graphites before and after heating for 1 h at 1200 °C are shown in Fig. 5 after correction for the carbon black used as a background. The major features of these spectra are due to water and CO_2, the main peak for CO (arrowed at 2143 cm^{-1}) was clearly not evident in any powder, confirming that its evolution above 780 °C was due to reaction between the adsorbed CO_2 and the carbon substrate. There are clear differences between the intensities of the peaks for the unmilled and 1000 h milled powders with both water and CO_2 being more intense in the longer milled powder. Thus, it seems clear that the longer milling

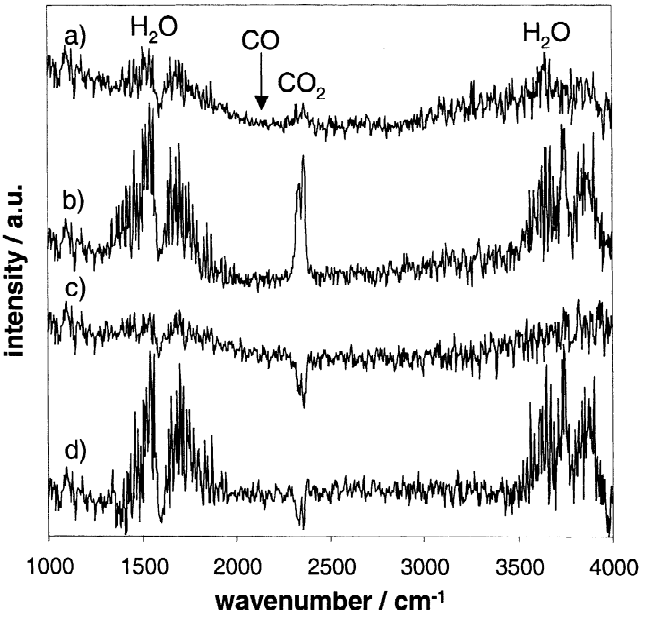

Fig. 5. Photoacoustic FTIR spectra of (a) unmilled, (b) 1000 h milled graphite, (c) and (d) are sample (a) and (b) heated for 1 h at 1200 °C in argon, respectively.

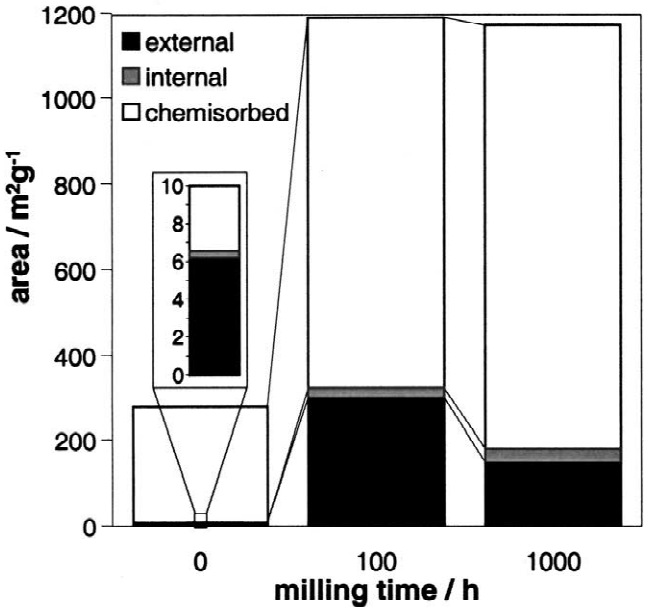

Fig. 6. Internal (micropore) and external surface areas of as-milled powders, the BET surface area is the sum of these two. The chemisorbed area was calculated according to the method in the text. The unmilled sample is also shown at a greater scale.

time leads to a greater quantity of adsorbed gas. After heating for 1 h at 1200 °C the spectra obtained showed a clear reduction in the CO_2 content, indeed both residual powders contained less CO_2 than the carbon black used as the background. The water contents differ with the 1000 h milled powder having a similar amount to that directly after milling, whereas the unmilled powder contained less. These results suggest that the sites where CO_2 was adsorbed were annealed out whereas those where water adsorbed did not. TGA of the annealed 1000 h sample showed a mass loss below 150 °C due to water and no further mass loss until 800 °C where a slow loss became evident.

Surface area measurements on the as-milled powders are shown in Fig. 6. The inset in Fig. 6 shows that the BET surface area of the unmilled powder (external + internal surface areas) was extremely small (6.5 $m^2\ g^{-1}$), with ~5% of this being internal porosity. This is slightly unexpected given the platy nature of graphite, Fig. 7(a, b), where the majority of the surface should be in the form of flat plates parallel to 002, which is the interlayer plane for graphite where easy cleavage occurs. The smaller particles evident were probably due to abrasion from the larger plates during handling and these comprise the majority of

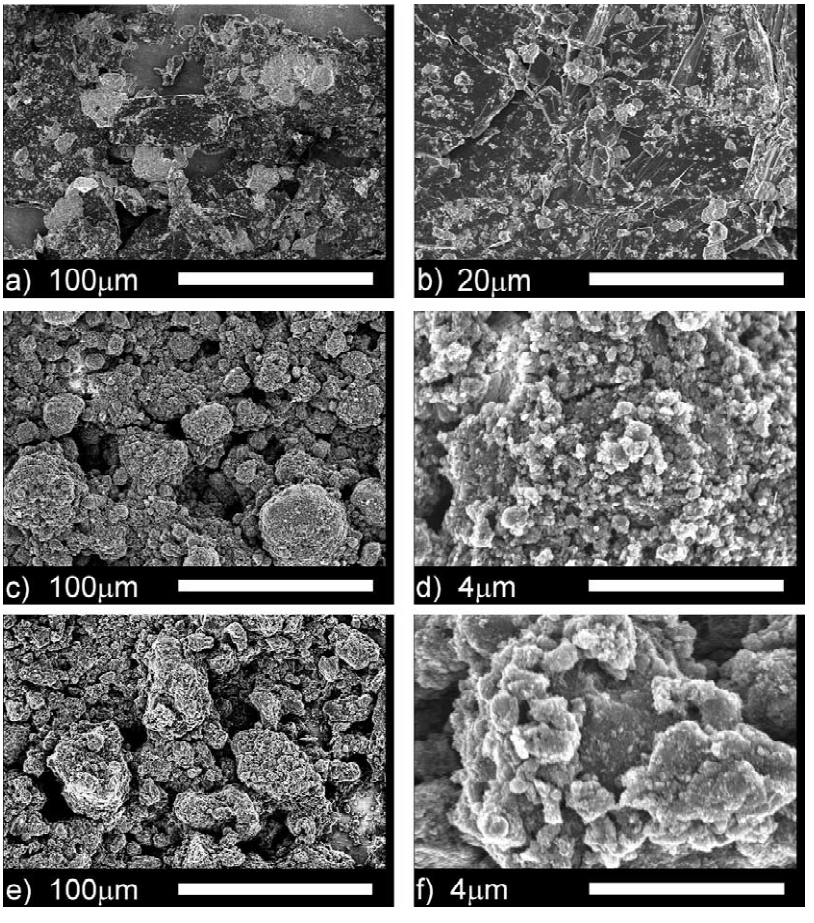

Fig. 7. Micrographs of (a, b) unmilled; (c, d) 100 h and (e, f) 1000 h milled graphite.

the surface area. The equivalent diameter of uniform graphite spheres with the same specific surface area was calculated to be ~0.43 μm which would confirm that the majority of the surface area was due to the smaller particles.

A massive increase in the BET surface area to 320 $m^2 g^{-1}$ was evident after 100 h of milling. The pore and external surface areas increasing approximately equally during this period with 7% of the total area being due to pores. The SEM images, Fig. 7(c, d), show that the range of particle sizes was much greater than in the unmilled powder and they were mostly rounded with no real evidence for the presence of facets, indicating that the large particles were agglomerates of smaller particles. A closer examination of the large particles showed that they were composed of <500 nm particles, some of which had faceting but the majority were rounded, indicating the loss of edges due to abrasion. It is not surprising that the external surface area measured increased dramatically after milling, especially when the graphite underwent the substantial size reduction evident in Fig. 7. The size of graphite spheres which would give the same external surface area (299 $m^2 g^{-1}$) is 9 nm, clearly all the particles evident are substantially larger than this and may indicate that the smaller particles are themselves agglomerates.

Therefore, the initial 100 h of milling led primarily to size reduction by fracture of the larger particles. The smaller particles are somewhat rounded implying that abrasion of corners and edges is also occurring leading to the very small particles evident in (d). The formation of significantly smaller particles is the major reason for the increased external surface area. The smaller particles formed would also be expected to be more highly strained and this was evident from analysis of the main XRD peak for the 002 plane at ~31° 2θ. This peak broadened indicating that the lattice strain increased from 0.30 to 0.44%.

Further milling to 1000 h led to only a slight increase in the lattice strain to 0.47% but a decrease in BET surface area to 178 $m^2 g^{-1}$. This decrease is due to an apparent drop in the external surface area to 146 $m^2 g^{-1}$ even though the pore surface increased to 32 $m^2 g^{-1}$. The SEM images of this powder, Fig. 7(e, f) do not show a substantial change compared with the 100 h milled graphite with the large particles being agglomerates of sub-micron particles.

Clearly, the BET technique does not appear to provide a true value for the surface area of these powders with a decrease in the external surface area apparent where an increase would be expected. The BET technique relies on the formation of a monolayer of gas on the surface of a solid [36] at low pressures. The general technique for measurement is to remove the adsorbed gas (usually by a combination of heating and evacuation) and then to adsorb nitrogen onto the gasless surface. However, if there is gas on the surface that is not removed during the pretreatment step a lower BET surface area results. If it is assumed that the mass loss above 200 °C was entirely due to the presence of adsorbed CO_2 (preparation for the BET measurement was made by heating to 200 °C); then from the mass loss above this temperature a value for the chemisorbed surface area can be estimated assuming a monolayer of CO_2. Taking the area of a carbon dioxide molecule to be 0.21 nm^2 [45,46], the absorbed gas areas were derived from the mass loss shown as squares in Fig. 2 and also shown in Fig. 6.

For all three powders there is a substantial area which is not investigated by BET. For the as-received powder 97.5% of the surface was not apparently measured by BET. Whether this area is external or pore is not known and may not be distinguishable, making any claims of nanoporosity [33] open to severe doubt. The total surface area including the chemisorbed CO_2 increased from 279 to 1188 after 100 h milling and 1169 $m^2 g^{-1}$ after 1000 h. The two areas for longer milling times are similar, and the data indicates that the chemisorbed area increased as the external surface area decreased. This is not unreasonable since the constant breaking and rewelding of particles during milling would lead to an activated surface which would be expected to be more susceptible to chemical bonding. This effect has been noted previously when some materials spontaneously combust in air directly after opening the mill. Similar transformations from external surface to chemisorbed surface have also been noted for milled activated carbon [47], although the total surface area did not change, the ratios of the various contributions did.

The apparent rewelding of particles which is evident in Fig. 7(c, e) may be, partially at least, due to binding of the carbon by iron abraded from the stainless steel balls and mill used. Indeed, heating of the 1000 h sample up to 1100 °C in argon showed the presence of one (or more) iron carbide phases. Previous work [17,18,31] has indicated that iron and graphite react during milling in a similar mill. After heating in air, haematite was the only iron phase present. An estimate of the iron content in the powders was made by ashing the carbon, deducting the mass of ash in the unmilled powder and assuming the residue was haematite (69.94 wt% Fe). The mass% of iron in the powder is shown in Table 2, and does not change substantially after the initial 100 h of milling, unlike activated carbon [47] where the longer milling times contained more iron.

Table 2
Mass of ash and derived iron content obtained by heating the milled graphite for 1 h at 1100 °C in air

Milling time/ h	Mass of ash/ mg g^{-1}	Fe content/ wt%
0	288	0.00 (assumed)
100	381	0.65
1000	378	0.63

Transmission electron micrographs of the sample milled for 100 h are shown in Fig. 8. It is clear from Fig. 8a that there are a significant number of ribbons up to 20 nm thick and 50 nm long in addition to the disordered material, these have been noted previously [7,48]. Closer examination of these ribbons (b, c and d) shows clear evidence of significant disruption to the ordered graphite structure with warping, delamination, dislocations and defects evident.

The expected regular laminar structure (an example of which is arrowed in d) is clearly absent from both (b and c). The inset in (b) shows a more detailed view which has clear defects and a significant degree of warping of the sheets with an almost complete absence of parallel planes. The approximate spacing between the planes is ~0.40 nm, substantially larger than for the starting graphite (0.3356 nm by X-ray diffraction) showing the expansion of the lattice. Towards the edge of the ribbon (inset in c) the interplanar spacing increases up to 0.50 nm, a massive increase on the starting material. The large range of interplanar spacings evident here (0.3356–0.50 nm) is reflected in the previously published [31] X-ray diffraction pattern where a broad peak centred around $d = 0.379$ nm ($2\theta = 27.33°$) was evident. The breadth of the peak is due to the wide distribution of d-spacings within the sample and is often taken to be a sign of a poorly ordered (amorphous) phase with a Scherrer crystallite size (coherence length) of <1 nm which is consistent with the TEM images.

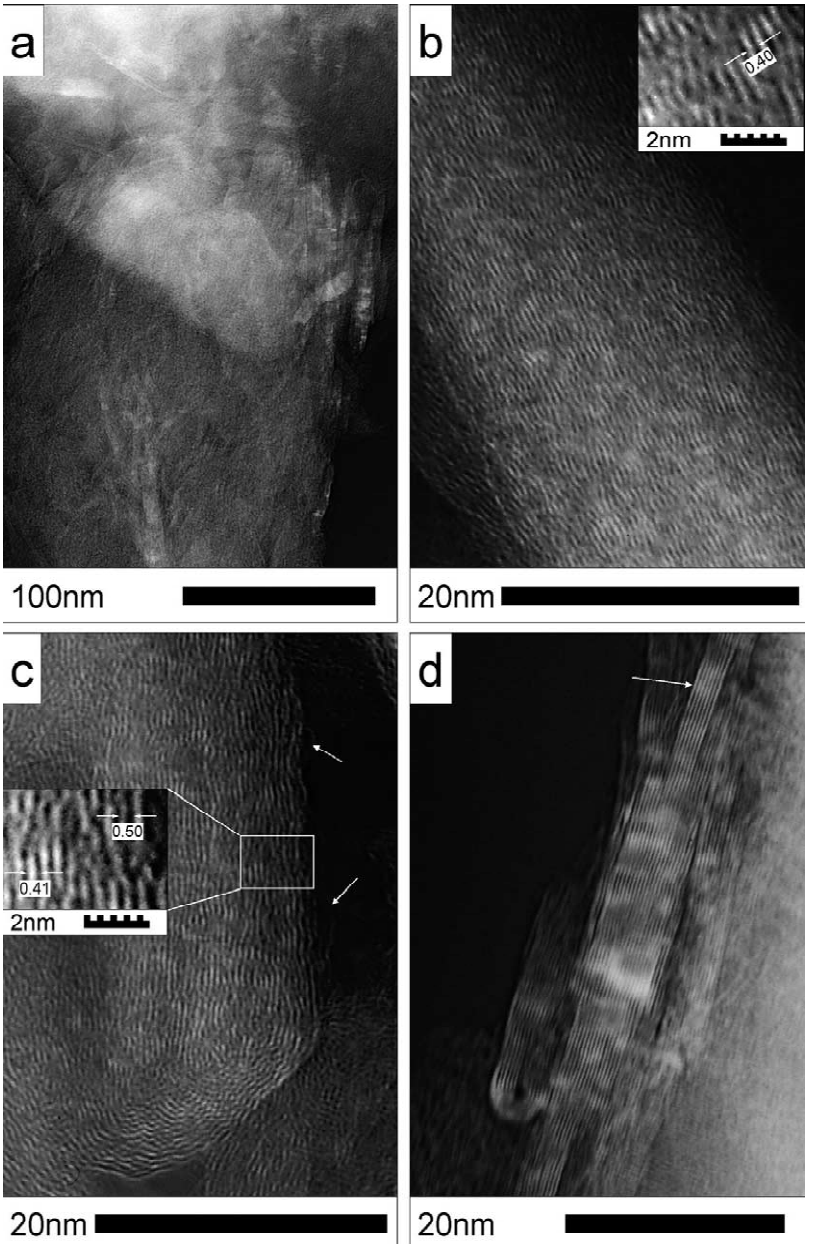

Fig. 8. Transmission electron micrographs of 100 h milled graphite.

There are some instances (arrowed in c) where single sheets of carbon atoms have been almost completely delaminated, this delamination does not seem to have been reported previously in milled powders, only as a constituent of arc-deposited fullerene-rich materials [49]. There is good evidence for the graphitic layers being bent through about 60° in (c), a range of angles has been noted previously [48] but not for such a large number of layers.

A half-loop is shown in (d) where six layers have been bent round through 180°. The diameter of the void in the centre of the loop is ~0.7 nm, which is essentially the same as that of a C_{60} molecule which may be the smallest diameter possible. The presence in the sample of such a fullerene-like structure may be the source of the Raman peak around 1473 cm^{-1}. However, the wide range of curved structures which are present would lead to a large range of Raman peaks, and the peak at 1473 cm^{-1} may well be due to one or more structures which are not evident in the TEM.

4. Conclusions

Ball milling of graphite for up to 1000 h in vacuum lead to the formation of a highly reactive carbon which was found to chemisorb large amounts of carbon dioxide after exposure to air. The presence of CO_2 on the surface was confirmed by FTIR and its removal during heating was demonstrated by TG–FTIR and FTIR of heated powders. The chemisorption was incomplete even after heating for 1 h at 1200 °C. BET surface area measurements indicated a maximum in the surface area after 100 h milling, however, the BET technique relies on a gas-free surface and the presence of chemisorbed gas leads to a gross underestimate of the true surface area. Even for the unmilled graphite the area covered by chemisorbed gas was around 40 times greater than the measured BET area. Milling led to an increase in the true surface area to ~1175 $m^2\ g^{-1}$ after both 100 and 1000 h; the major difference between the powders being an increase in the ratio of chemisorbed gas area to the BET area. These results show that use of the BET technique for milled powders is potentially very misleading, especially when the powder becomes highly chemically active towards exposure to active gas atmospheres such as air or oxygen.

Raman spectroscopy of the powders showed a decrease in the crystallinity of the graphite with milling time and an increase in the diamond-like sp^3 and fullerene-like bonding in the sample. TEM of the 100 h powder showed the presence of ribbons up to 20 nm thick and 50 nm long. These ribbons comprised few examples of true graphitic structure with defects, delamination, translation, warping and curvature all evident. Examples of curved partly delaminated single sheets were evident as were loops with a minimum diameter of ~7 nm. The interplanar spacings were ~0.40 nm, somewhat larger than unmilled graphite and towards the edges of the ribbons increased up to ~0.50 nm.

Acknowledgements

The authors would like to thank David Llewellyn of the Department of Electronic Materials Engineering and the Electron Microscope Unit at the Australian National University for his invaluable aid and expertise in taking the TEM images. Valuable comments were made by Dr Andrei Rode, Dr Vincent Craig and Dr Andrew Christy, all of the Research School of Physical Sciences and Engineering at the Australian National University.

References

[1] K. Niwase, T. Tanaka, Y. Kakimoto, K.N. Ishihara, P.H. Shingu, Mater. Trans. JIM 36 (1995) 282.
[2] T.D. Shen, W.Q. Ge, K.Y. Wang, M.X. Quan, J.T. Wang, W.D. Wei, C.C. Koch, Nanostructured Mater. 7 (1996) 393.
[3] J. Tang, W. Zhao, L. Li, A.U. Falster, W.B. Simmons, W.L. Zhou, Y. Ikuhara, J.H. Zhang, J. Mater. Res. 11 (1996) 733.
[4] W.L. Zhou, Y. Ikuhara, W. Zhao, J. Tang, Carbon 33 (1995) 1177.
[5] J.B. Aladekomo, R.H. Bragg, Carbon 28 (1990) 897.
[6] M. Nakamizo, H. Honda, M. Inagaki, Carbon 16 (1978) 281.
[7] T.S. Ong, H. Yang, Carbon 38 (2000) 2077.
[8] H. Hermann, T. Schubert, W. Gruner, N. Mattern, Nanostructured Mater. 8 (1997) 215.
[9] E. Kasai, K. Mae, F. Saito, ISIJ Int. 35 (1995) 1444.
[10] H. Yang, G. Nguyen, P.G. McCormick, Scripta Metall. Mater. 32 (1995) 681.
[11] N.J. Welham, Miner. Eng. 9 (1996) 1189.
[12] N.J. Welham, CIM Bull. 90 (1997) 64.
[13] N.J. Welham, Proc. Australasia. Inst. Mining Metall 302 (1997) 61.
[14] P. Matteazzi, G. Le Caer, J. Am. Ceram. Soc. 74 (1991) 1382.
[15] Z.G. Liu, J.T. Guo, L.L. Ye, G.S. Li, Z.Q. Hu, Appl. Phys. Lett. 65 (1994) 2666.
[16] G.M. Wang, P. Millet, A. Calka, S.J. Campbell, Mater. Sci. Forum 179–181 (1995) 183.
[17] G.M. Wang, S.J. Campbell, A. Calka, W.A. Kaczmarek, Nanostructured Mater. 6 (1995) 389.
[18] S.J. Campbell, G.M. Wang, A. Calka, W.A. Kaczmarek, Mater. Sci. Eng. A 226 (1997) 75.
[19] N.J. Welham, J. Mater. Res. 14 (1999) 619.
[20] N.J. Welham, J. Am. Inst. Chem. Eng 46 (2000) 68.
[21] N.J. Welham, Metall. Trans. A 31 (2000) 283.
[22] K. Tkacova, P. Balaz, Int. J. Mineral Proc. 44–45 (1996) 197.
[23] K. Tkacova, V. Sepelak, N. Stevulova, V.V. Boldyrev, J. Solid State Chem. 123 (1996) 100.
[24] P. Balaz, Hydrometallurgy 40 (1996) 359.
[25] T. Puclin, W.A. Kaczmarek, B.W. Ninham, Mater. Chem. Phys. 40 (1995) 73.
[26] N.J. Welham, D.J. Llewellyn, Miner. Eng. 11 (1998) 827.
[27] N.J. Welham, Int. J. Miner. Proc. 61 (2000) 145.
[28] P. Balaz, M. Balassaova, J. Therm. Anal. 41 (1994) 1101.
[29] P. Balaz, J. Briancin, Solid State Ionics 63–65 (1993) 296.
[30] N.J. Welham, Can. Metall. Q. 40 (2001) 143.
[31] N.J. Welham, J.S. Williams, Carbon 36 (1998) 1309.
[32] F. Disma, L. Aymard, L. Dupont, J.M. Tarascon, J. Electrochem. Soc. 143 (1996) 3959.

[33] Y. Chen, J.F. Gerald, L.T. Chadderton, L. Chaffron, Appl. Phys. Lett. 74 (1999) 2782.
[34] A. Calka, A.P. Radlinski, Mater. Sci. Eng. A134 (1991) 1350.
[35] W.D. Harkins, G. Jura, J. Chem. Phys. 11 (1943) 431.
[36] S. Brunauer, P.H. Emmett, E. Teller, J. Phys. Chem. 60 (1938) 309.
[37] M. Endo, C. Kim, T. Karaki, T. Tamaki, Y. Nishimura, M.J. Matthews, S.D.M. Brown, M.S. Dresselhaus, Phys. Rev. B: Condensed Matter 58 (1998) 8991.
[38] V.I. Merkulov, J.S. Lannin, C.H. Munro, S.A. Asher, V.S. Veerasamy, W.I. Milne, Phys. Rev. Lett. 78 (1997) 4869.
[39] J. Schwan, S. Ulrich, V. Batori, H. Ehrhardt, S.R.P. Silva, J. Appl. Phys. 80 (1996) 440.
[40] C.Z. Wang, K.M. Ho, Phys. Rev. Lett. 71 (1993) 1184.
[41] P.C. Eklund, J.M. Holden, R.A. Jishi, Carbon 33 (1995) 959.
[42] A.V. Rode, E.G. Gamaly, B. Luther-Davies, Appl. Phys. A: Mater. Sci. Process. 70 (2000) 135.
[43] N.R. Laine, F.J. Vastola, P.L. Walker Jr., J. Phys. Chem. 67 (1963) 2030.
[44] H. Harker, J.B. Horsley, D. Robson, Carbon 9 (1971) 1.
[45] A.L. McClellan, H.F. Harnsberger, J. Colloid Interf. Sci. 23 (1967) 577.
[46] C.U. Pittman, W. Jiang, Z.R. Yue, C.A.L.Y. Leon, Carbon 37 (1999) 85.
[47] N.J. Welham, V. Berbenni, P.G. Chapman, Carbon 40 (2002) 2307.
[48] X.H. Chen, H.S. Yang, G.T. Wu, M. Wang, F.M. Deng, X.B. Zhang, J.C. Peng, W.Z. Li, J. Cryst. Growth 218 (2000) 57.
[49] L.N. Bourgeois, L.A. Bursill, Philos. Mag. A 76 (1997) 753.